

## Wavelength Dependence of LAB+PPO Emission Time

---

Tanner Kaptanoglu,<sup>a,1</sup> Josh Klein,<sup>a</sup> Meng Luo<sup>a</sup>

<sup>a</sup>University of Pennsylvania,  
209 South 33rd Street Philadelphia PA 19104, USA

E-mail: [tannerk@hep.upenn.edu](mailto:tannerk@hep.upenn.edu)

**ABSTRACT:** Linear alkyl benzene (LAB) has in recent years been used as a solvent for PPO in large-scale scintillation detectors, like Daya Bay and SNO+. The combination has several nice properties, including high light yield, good materials compatibility, and excellent pulse shape discrimination. As charged particles move through the LAB+PPO, both Cherenkov and scintillation light are created. Separating Cherenkov from scintillation light would allow a broad range of physics in future large-scale detectors like THEIA [1], by allowing direction reconstruction with Cherenkov light while retaining the high light yield and good particle ID of a scintillator detector. In this paper, we examine the discrimination of Cherenkov and scintillation light using a set of bandpass filters. In principle, Cherenkov light should extend beyond the wavelength band of the PPO emission spectrum, allowing exclusive identification. We have found that in fact the PPO emission extends well beyond 500 nm but, surprisingly, the long wavelength light from PPO is significantly delayed compared to the shorter wavelength PPO emission. The delay allows us to identify Cherenkov emission distinct from the scintillation light.

**KEYWORDS:** Cherenkov detectors, Scintillators, scintillation and light emission processes (solid, gas and liquid scintillators), Neutrino detectors, Detectors for UV, visible and IR photons, Attenuators, Filters

---

<sup>1</sup>Corresponding Author.

---

## Contents

<b>1</b>	<b>Introduction</b>	<b>1</b>
<b>2</b>	<b>Experimental Setup</b>	<b>2</b>
<b>3</b>	<b>Data Analysis</b>	<b>4</b>
<b>4</b>	<b>Results</b>	<b>5</b>
<b>5</b>	<b>Discussion</b>	<b>7</b>
<b>6</b>	<b>Conclusion</b>	<b>9</b>
<b>7</b>	<b>Acknowledgements</b>	<b>9</b>
<b>A</b>	<b>Panel of Timing Spectra</b>	<b>10</b>
<b>B</b>	<b>Fit Parameter Plots</b>	<b>11</b>

---

## 1 Introduction

Several large-scale neutrino experiments use liquid scintillator targets to achieve a high light yield and excellent pulse-shape discrimination. Some of these experiments, as well as future experiments, rely on Linear alkyl benzene (LAB) as the primary solvent in a scintillator cocktail [2–4] that often includes PPO as a primary fluor. In a large-scale detector like SNO+ or Daya Bay, the wavelength profile of the PPO (and any additional secondary fluors) plays an important role in the detector’s overall light yield, because non-trivial amounts of scattering and absorption affect the number and spectrum of photons reaching the photon detectors (photomultiplier tubes or other devices).

Future large-scale scintillation experiments like THEIA [1] plan to detect both Cherenkov and scintillation light as a way of providing a very broad range of physics with a single detector. Cherenkov light allows direction reconstruction which can aid in identifying solar neutrino events [5], identification of neutrinoless beta decay candidates against the solar neutrino [6] background, or discrimination of high-energy  $\nu_e$  events from  $\pi^0$ s, which is important for studying long-baseline neutrino oscillations. The scintillation light provides a high light yield that is critical for good energy and position reconstruction. The time profile of the scintillation light is also important, because it affects position reconstruction and provides ways of discriminating particles like  $\beta$ s from  $\alpha$ s. The emission time profile has already been well characterized on the bench-top by several experiments including SNO+, Daya Bay, LENA, and Borexino [7–10]. Separation of Cherenkov and scintillation light using the difference in timing and the directionality of the Cherenkov light was demonstrated very nicely in Refs. [11–13].

Another approach for discriminating Cherenkov from scintillation light is to look in different wavelength bands. Cherenkov light is much broader, peaking in the UV and falling off like  $\lambda^{-2}$ , while scintillation light typically has a narrow-band spectrum. Thus, by selecting long wavelength light, either using filters or red-sensitive photon detectors [11], we anticipate an ability to detect some Cherenkov photons without contamination from scintillation light.

A critical requirement for this is that the scintillator emission spectrum is very small at long wavelengths, so that the Cherenkov light is not hidden. LAB+PPO would therefore seem like an ideal cocktail: its spectrum is believed to span a relatively narrow band of wavelengths, ranging from about 350 to 450 nm. We find in this paper, however, that beyond 500 nm there is still PPO emission at a level that is competitive with the level of Cherenkov light but that, surprisingly, the long wavelength emission is significantly delayed relative to the Cherenkov light and to the short wavelength scintillation light. Thus, identification of the Cherenkov light is still very clean, even though there is scintillation light present at long wavelengths. We provide here curves showing the time profiles for a series of wavelength bands, and the apparent delay as a function of the central wavelength of each band. The time-delayed long wavelength light appears to be a distinct process, and not part of a continuum of time delays from short-to long wavelengths. We know of no other measurements that show this delay at long wavelengths.

## 2 Experimental Setup

A diagram of the experimental setup is shown in Figure 1. The setup consists of a  $^{90}\text{Sr}$   $\beta^-$  source deployed above a hollowed out UV-transparent acrylic block. The block is a 3 x 3 x 3.5 cm cube with a machined out cylindrical volume that is 2 cm in diameter. That volume is filled with LAB+PPO scintillator. The PPO is added at a concentration of 2g/L to the LAB. Dissolved oxygen, which has previously been shown to impact the time profile of the scintillation light [8], was not removed from the scintillator. The majority of the effect is the removal of some quenching for the late-time scintillation light, but the first time-constant was not significantly changed, which is the primary concern for this paper.

The  $^{90}\text{Sr}$  undergoes a 0.546 MeV  $\beta^-$  decay to  $^{90}\text{Y}$  with a half life of 29.1 years. The  $^{90}\text{Y}$  undergoes a 2.28 MeV  $\beta^-$  decay to  $^{90}\text{Zr}$  with a half-life of 64 hours. The  $\beta^-$  particles enter the scintillator and create isotropic scintillation light. In addition, the  $\beta^-$  particles create Cherenkov light in the scintillator, and some enter the acrylic block creating additional Cherenkov light there. At these low energies the  $\beta^-$  particles often undergo several scatters such that the Cherenkov light can be created traveling in any direction. The light yield of the scintillation light is about 10,000 photons per MeV [12], compared to around 300 photons per MeV for Cherenkov light in the wavelength band detectable by photomultiplier tubes.

A Hamamatsu super-bialkali R7600-U200 PMT is optically coupled to the acrylic block using Saint-Gobain BC-630 optical grease. The PMT acts as a high efficiency fast trigger and provides the time-zero. The efficiency curve of the PMT, shown in Figure 2, spans a broad range of wavelengths and can thus be used for all of the measurements described in this paper. On the other side of the source, 5 cm from the trigger PMT, is a mask with a small aperture, 1 cm in diameter. The center of the aperture is 3 cm above the base of the acrylic block. Directly behind the aperture we place a series of bandpass filters that absorbs light outside a small band of wavelengths. The size

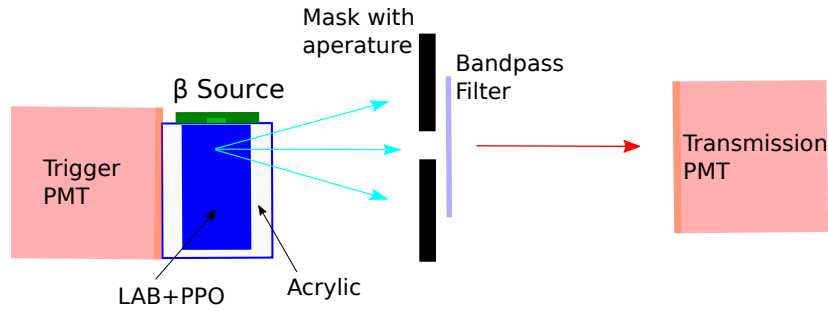


**Figure 1.** A schematic of the experimental setup, showing the  $\beta$  source deployed above the LAB+PPO target and the locations of the mask, PMTs, and bandpass filter.

of the aperture ensures that the transmission PMT detects primarily single photons. That light is viewed by a second R7600-U200 PMT, placed 15 cm from the mask, which is used to measure the transmitted light over the wavelengths passed by the filter. This low coincidence rate technique follows the single photon counting method described in [14]. Both PMTs are operated at -800V where their gains are approximately  $5 \times 10^6$ .

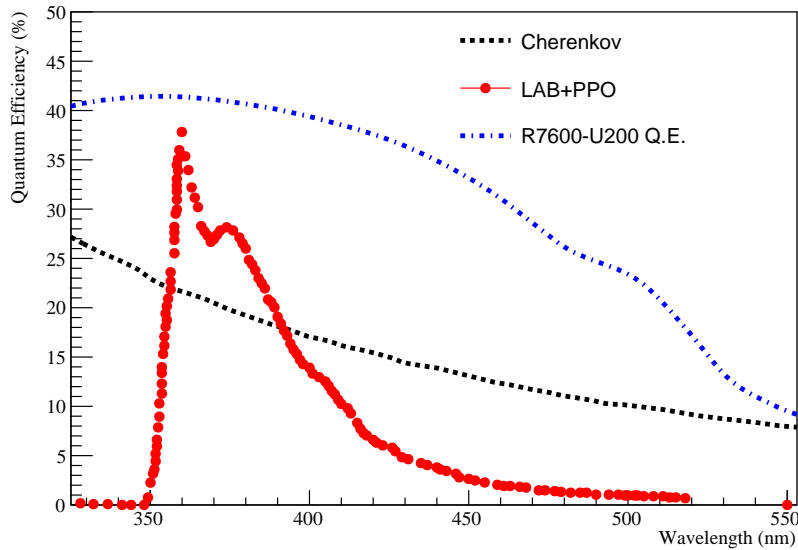


**Figure 2.** The wavelength spectrum of Cherenkov light, LAB+PPO scintillation light, and the R7600-U200 PMT quantum efficiency (Q.E.). The PPO emission spectrum shown includes self-absorption. The PPO and Cherenkov spectrum are scaled arbitrarily and show shape only. The Q.E. curve is provided by Hamamatsu [16] and peaks above 40% in quantum efficiency.

Our data acquisition system includes a Lecroy WaveRunner 606Zi 600 MHz oscilloscope, which is used to digitize the signals from both PMTs. Waveforms are sampled every 100 ps for 500 ns. The oscilloscope has an 8-bit ADC with a variable dynamic range, which allows for roughly 100

$\mu\text{V}$  resolution. The LeCrunch software [15] is used to read out the data from the oscilloscope over Ethernet as well as format the data into custom HDF5 files. The emission spectrum of the LAB+PPO is measured using a UV-Vis Ocean Optics Spectrometer by directly exciting the scintillator with a 335 nm LED. The measurement is made by placing the spectrometer at the same relative location as the aperture to probe the spectrum of light that the transmission PMT will view. The scintillator for this measurement is held in the same acrylic block. The measured spectrum is shown in Figure 2 and includes effects from self-absorption, described in more detail in [17]. As can be seen in the figure, there is small, but non-zero emission, above 500 nm.

The bandpass filters that are used in this measurement are shown in Table 1. A set of filters are chosen to span across the emission spectrum of LAB+PPO. Data provided by Thorlabs and Edmund Optics [18, 19] indicates that the transmission is less than 0.01% outside of the pass band of the filters. In all cases the filter is placed normal to the light coming from the aperture, so that the average incident angle at the filter is  $0^\circ$ .

Center (nm)	FWHM (nm)	Peak Transmission (%)
$355 \pm 2$	10	95
$387 \pm 3$	11	95
$405 \pm 2$	10	96
$430 \pm 2$	10	46
$450 \pm 2$	10	98
$470 \pm 2$	10	53
$494 \pm 3$	20	95
$510 \pm 2$	10	60
$530 \pm 2$	10	54

**Table 1.** The center wavelength, FWHM, and transmission at the central wavelength for each of the bandpass filters. Data is provided by Thorlabs and Edmund Optics [18, 19].

### 3 Data Analysis

Offline analysis code is used to find coincidences between the trigger and transmission PMTs. A software-based constant fraction discriminator is used to find the time difference between the trigger PMT and the transmission PMT signals. A very low coincidence rate of less than 3% ensures that the transmission PMT is detecting primarily single photons. The  $\Delta t$  between the trigger and transmission PMT crossing is histogrammed. The only event selection criterion is a lower charge cut on the trigger PMT to ensure the triggered event corresponds to the  $\beta^-$  particle traveling through the scintillator.

Another particularly nice feature of the R7600-U200 PMTs is the negligible amounts of pre-pulsing, late-pulsing, and dark-pulsing [20]. The dark count rate of the PMTs is around 50 Hz and is uncorrelated with the trigger time. As a result the contribution from dark counts to the  $\Delta t$  histogram is insignificant, which is confirmed for each data set by looking in a window before the trigger. Because the trigger rate from the  $\beta^-$  source is approximately 1 kHz, contributions are minor

from backgrounds such as cosmic muons through the scintillator volume, which was confirmed by taking data with no source.

## 4 Results

Data was taken for nine different bandpass filters with distinct central transmission wavelengths, shown in Table 1. The scintillation time profile is constructed for each data set using the methods described in Section 3. Less data was necessary for the shorter wavelength bandpass filters to achieve roughly the same level of statistics as the longer wavelength filters. In general, sufficient data was taken for each filter until the statistical uncertainties were smaller than 3% in the peak of the emission spectrum. The 3% level ensures that the rise times of the time profiles can be clearly distinguished.

Ten data sets were taken, including one with no bandpass filter. Figure 3 shows the scintillation emission profile for each data set. The histograms are normalized to the peak of the scintillation light to show how the shape of the profile changes with wavelength. A clear shift in the scintillation light is observed for the longer wavelength filters above 430 nm. For example, in the 494 nm filter data the peak has shifted about 3 ns from the location of the peak in 355 nm filter data. Additionally, at these long wavelengths, the Cherenkov component of the light can be clearly seen peaking at early times. Note the absolute time offset is arbitrary due to various cable delays and transit times, but the Cherenkov light provides a very useful  $t_0$  for the various samples.

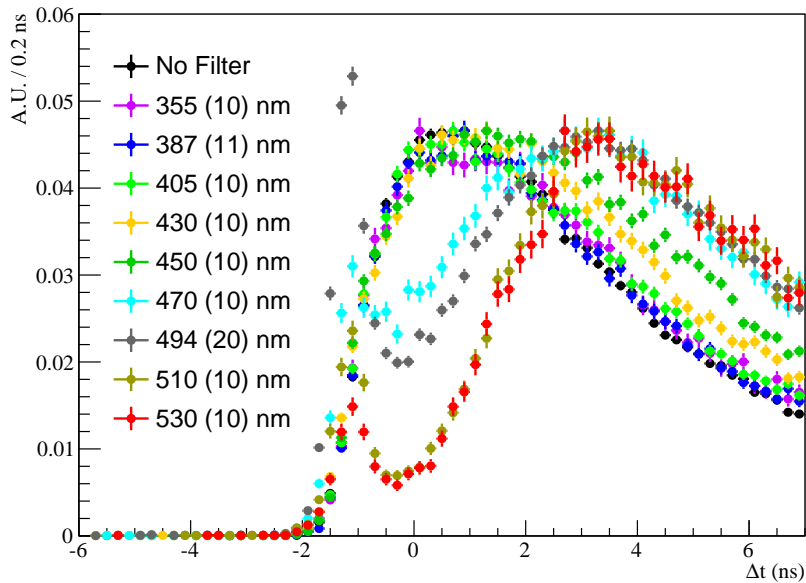


**Figure 3.** The time emission profile, zoomed into the rise time of the LAB+PPO for different wavelength regimes. The light is selected using the bandpass filters listed in Table 1. The central wavelength and width of the bandpass filters are specified in the legend. The histograms are normalized to the peak of the scintillation light to illustrate shape differences. The Cherenkov light can be clearly identified at early times in the data for the filters longer than 450 nm. The data for each filter is separated into individual panels in Figure 6.

The spectra are fit to Equation 4.1 using the RooFit package [21]. The scintillation light is fit to the sum of two decay exponentials with time constants  $\tau_1$  and  $\tau_2$ , weights  $A_1$  and  $A_2$ , and an exponential rise time,  $\tau_R$ . The weights  $A_1$  and  $A_2$  are constrained to sum to one. The PMT transit time spread (TTS) is determined offline using a Cherenkov light source to be 350 ps, which is in good agreement with the Hamamatsu datasheet. Additionally,  $f_{PMT}$  accounts for the TTS of both the trigger and transmission PMT. That model,  $f_{PMT}$  is convolved with the scintillation profile. An offset  $t'$  allows for cable delays and other arbitrary time offsets. The second component of the model accounts for the Cherenkov light, which is modeled simply as  $f_{PMT}$  because the Cherenkov light is emitted promptly in comparison to the TTS of the PMTs. The scintillation and Cherenkov light are weighted appropriately by  $C$ . The fit allows for a different time offset for the Cherenkov and scintillation light due to the empirical observation that the scintillation light can be additionally delayed.

$$F = C \times f_{PMT}(t - t'') + (1 - C) \times \sum_{i=1}^2 \frac{A_i \times (e^{-t/\tau_i} - e^{-t/\tau_r})}{(\tau_i - \tau_r)} * f_{PMT}(t - t') \quad (4.1)$$

Equation 4.2 defines the  $\Delta T$  parameter, which is the difference in time between the the Cherenkov and scintillation peaks. This difference is offset to zero for the data with no filter by adjusting the constant  $t_{nf}$ . This is done to make clear the additional delay incurred for the long wavelength filters.

$$\Delta T = t' - t'' - t_{nf} \quad (4.2)$$

The full scintillation spectrum is typically fit with three or four exponential decay time constants. Our primary goal here, however, is to identify how the early time component of the scintillation light changes with wavelength, and thus only the first 30 ns of the spectrum are fit. Neither the length of the waveform nor the length of data taking provides for accurate measurement of the full scintillation spectrum, which has already been measured by several experiments. Figure 4 shows two examples of the fit with the Cherenkov and scintillation components separated.

One can select a relatively pure sample of Cherenkov light by integrating the time profile in a prompt window. Equation 4.3 defines the purity,  $P$ , of the Cherenkov light in a prompt window, where  $F_C$  is the Cherenkov component in the fit. The upper and lower bounds of the integral are taken to span the Cherenkov component (Figure 4) and are arbitrarily offset from zero based on cable delays and other time offsets.

Some of the Cherenkov light detected in our setup comes from  $\beta$ s that enter the acrylic cube after depositing some energy in the scintillator. We have used a GEANT4-based Monte Carlo to estimate the size of this effect, and have found that removing the acrylic block from the simulation reduces the fraction of Cherenkov light by up to 40%. We take this as an overall systematic uncertainty on our numbers; a complete correction would rely on a more detailed simulation model.

$$P = \int_{8.0}^{10.0} \frac{F_C}{F} dt \quad (4.3)$$

Table 2 shows the full fit results for the ten data sets. The time constants and their relative fractions ( $\tau_1$ ,  $\tau_2$ , and  $A_1$ ) are consistent across a wide range of wavelengths. This suggests that the

scintillation light in each wavelength regime is being produced via the same mechanism. Both the rise time and the shift to the peak increase as the wavelength gets longer.

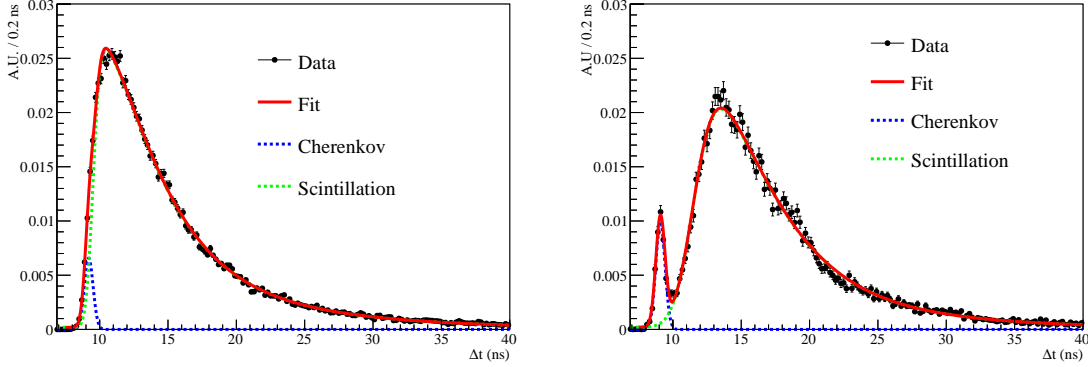


**Figure 4.** The full fit for the 355 nm bandpass filter data (left) and 510 nm bandpass filter data (right) is shown in red. The Cherenkov and scintillation components of the fit are shown explicitly.

Filter	$A_1$ (%)	$\tau_R$ (ns)	$\tau_1$ (ns)	$\tau_2$ (ns)	$1 - C$ (%)	$\Delta T$ (ns)	$P$ (%)
None	$68 \pm 3$	$1.6 \pm 0.1$	$3.6 \pm 0.1$	$10.8 \pm 1.8$	$98 \pm 2$	$0.00 \pm 0.00$	$29 \pm 4$
355	$71 \pm 4$	$1.8 \pm 0.1$	$3.6 \pm 0.1$	$10.5 \pm 1.8$	$97 \pm 2$	$0.02 \pm 0.02$	$23 \pm 4$
387	$73 \pm 4$	$1.8 \pm 0.1$	$3.7 \pm 0.1$	$10.8 \pm 1.8$	$98 \pm 2$	$-0.01 \pm 0.02$	$28 \pm 4$
405	$64 \pm 3$	$1.7 \pm 0.1$	$3.6 \pm 0.1$	$9.3 \pm 2.0$	$97 \pm 2$	$0.03 \pm 0.02$	$33 \pm 4$
430	$66 \pm 3$	$1.9 \pm 0.1$	$3.7 \pm 0.1$	$9.6 \pm 1.8$	$96 \pm 2$	$0.12 \pm 0.02$	$41 \pm 4$
450	$69 \pm 3$	$2.2 \pm 0.1$	$3.9 \pm 0.2$	$10.8 \pm 2.2$	$94 \pm 2$	$0.17 \pm 0.02$	$48 \pm 4$
470	$70 \pm 4$	$2.4 \pm 0.2$	$3.8 \pm 0.2$	$11.2 \pm 2.4$	$95 \pm 2$	$0.80 \pm 0.04$	$66 \pm 4$
494	$71 \pm 3$	$2.4 \pm 0.1$	$4.0 \pm 0.2$	$12.5 \pm 2.0$	$92 \pm 2$	$1.22 \pm 0.02$	$74 \pm 4$
510	$72 \pm 4$	$2.3 \pm 0.3$	$3.6 \pm 0.3$	$10.6 \pm 2.4$	$95 \pm 2$	$1.93 \pm 0.06$	$85 \pm 4$
530	$79 \pm 6$	$2.2 \pm 0.3$	$3.6 \pm 0.4$	$13.3 \pm 3.0$	$97 \pm 3$	$2.08 \pm 0.10$	$81 \pm 5$

**Table 2.** The fit results for each of the bandpass filters. The fit parameters are shown in Equation 4.1.  $\Delta T$  is defined in Equation 4.2 and  $P$  is defined in Equation 4.3. Several of the parameters are plotted against wavelength in Figure 7.

The amount of scintillation light for each bandpass filter can be compared to what is expected based on the measured emission spectrum. In order to do so, the total amount of scintillation light per triggered event is scaled based on the expected transmission of the filter and efficiency of the PMT. The result is shown in Figure 5, compared directly to the measured emission spectrum. The bandpass filter data is consistent with our measured emission spectrum, including the long wavelength emission beyond 500 nm.

## 5 Discussion

The long wavelength PPO emission appears to be associated with a process that is distinct from the standard PPO emission. As can be seen even as low as 430 nm, light that is delayed begins to appear

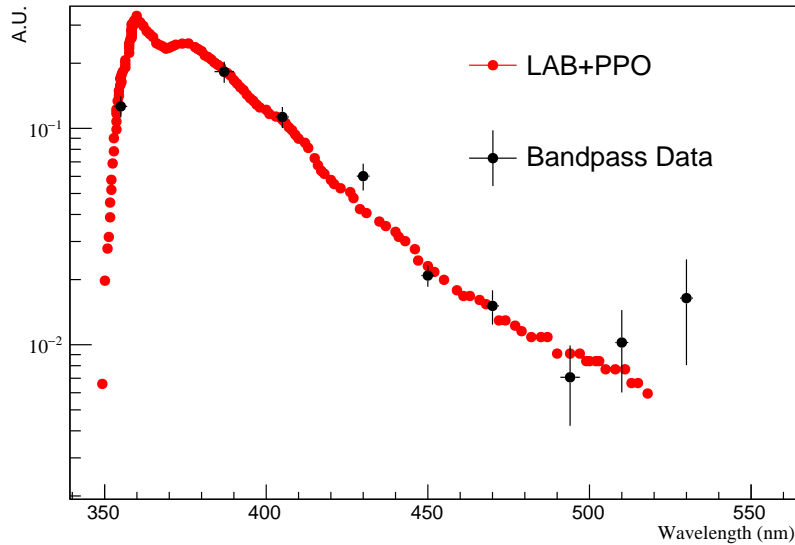


**Figure 5.** The measured emission spectrum compared to the amount of scintillation light detected for each bandpass filter. The amount of scintillation light is scaled based on the total number of triggered events, the efficiency of the PMT, and the transmission of the filter. The shape extracted from the bandpass filter measurement agrees well with the emission spectrum.

and by the time the the bandpass gets to 500 nm almost all the light is shifted. The delay is fortunate from the standpoint of discriminating Cherenkov and scintillation light, as our fits demonstrate.

This delayed long wavelength PPO emission does not appear to be caused by self-absorption and re-emission. To demonstrate more clearly, the PPO concentration was increased to 4 g/L which halves the absorption length but only increases the intrinsic light output by 10% [22]. Using the 530 nm bandpass filter, the amount of scintillation light detected increased by 10%, inconsistent with a model where the long wavelength light is being produced via self-absorption/reemission.

In general the LAB transfers its energy to the PPO non-radiatively; however, a small amount of the light is directly emitted by the LAB. This long wavelength light is not from the direct LAB emission, which produces light at shorter wavelength than the PPO [23]. To check this, data was taken with LAB without PPO and no scintillation light was detected using the 494 nm bandpass filter.

In a large-scale detector, we first expect the fraction of Cherenkov light to likely be smaller than our measurements, because of our “contamination” from Cherenkov light in the acrylic block. But one positive aspect of looking at long wavelength light as a way of identifying Cherenkov light is that the long wavelength photons travel faster in scintillator than short wavelength photons, making identification via timing, like that in Ref. [11], easier. In addition, scattering—which can spoil the directionality of the Cherenkov photons—is reduced at long wavelengths.

## 6 Conclusion

Using bandpass filters to look at specific segments of the LAB+PPO emission spectrum has demonstrated that the long wavelength scintillation light is delayed relative the short wavelength scintillation light. Empirically there appear to be two distinct processes. The standard process contributes primarily around 360 nm and makes up the bulk of the emission, which is what has been measured in previous efforts. However, this paper has demonstrated that there is (at least) one scintillation process that contributes at long wavelengths and has a much slower rise-time. This process dominates above 500 nm, as indicated in the 510 and 530 nm bandpass filter data.

Practically, this makes using wavelength to separate Cherenkov from scintillation light easier. For the bandpass filters above 450 nm, placing a prompt cut allows one to select a pure sample of Cherenkov light, primarily because of the slow rise of the long wavelength scintillation light. This feature is useful for future Cherenkov and scintillation separation studies using LAB+PPO.

## 7 Acknowledgements

Thanks to Gabriel Orebi Gann for helpful discussion about Cherenkov/scintillation separation and future application with THEIA. Thanks to Ian Coulter, Eric Marzec, Logan Lebanowski, and Nuno Barros for useful discussion regarding the LAB+PPO timing and emission spectra. Thanks to Tony LaTorre for developing the Lecrunch software used for the data readout and for suggestions regarding fitting the timing spectrum. This work was supported by the Department of Energy and the Office of High Energy Physics, under grant number DE-FG02-88ER40479.

## A Panel of Timing Spectra

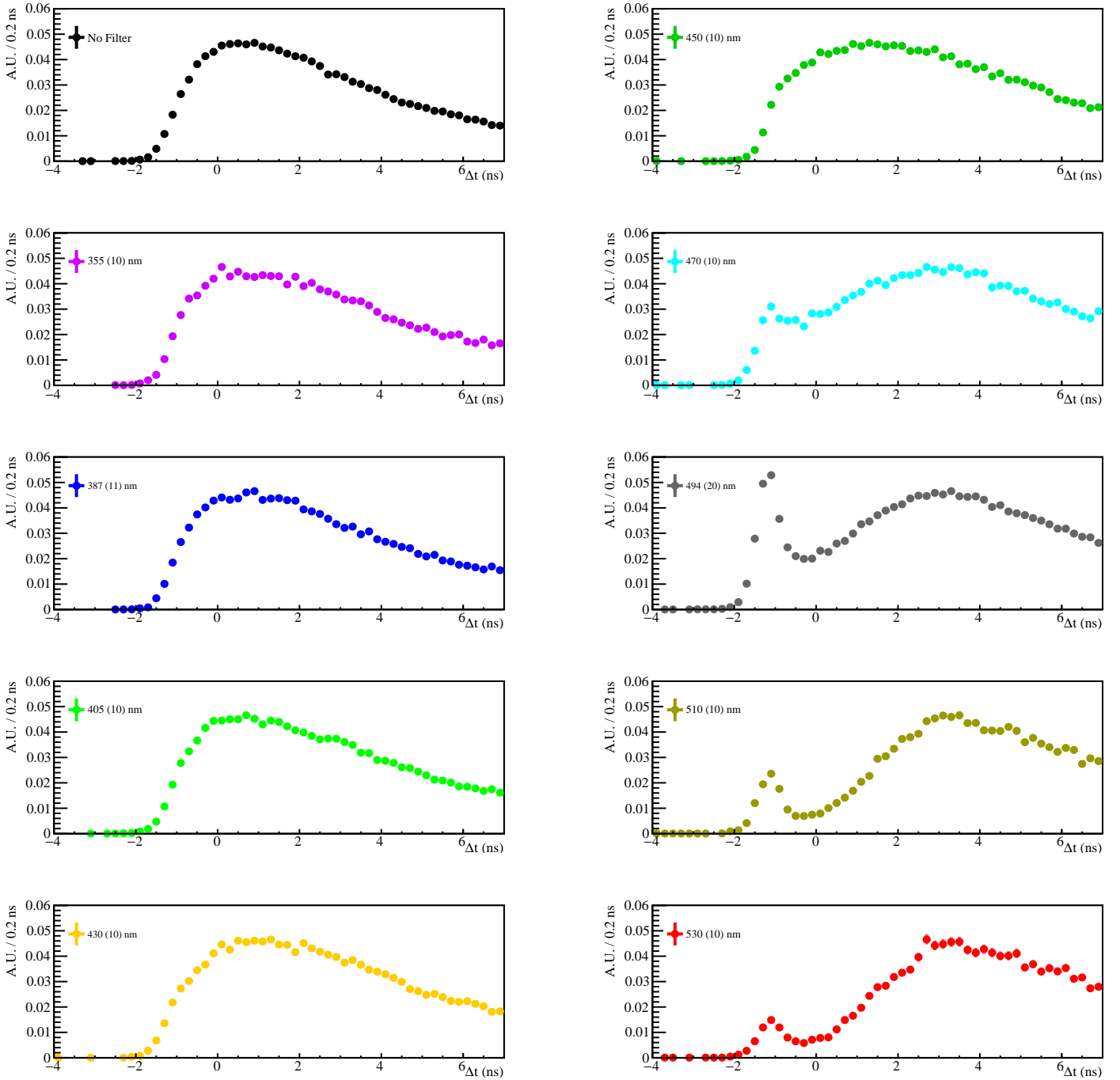


**Figure 6.** The time emission profile, zoomed into the rise time of the LAB+PPO for different wavelength regimes. The light is selected using the bandpass filters listed in Table 1. This plot shows the same data as Figure 3, but with the data for each bandpass filter separated by panel.

## B Fit Parameter Plots

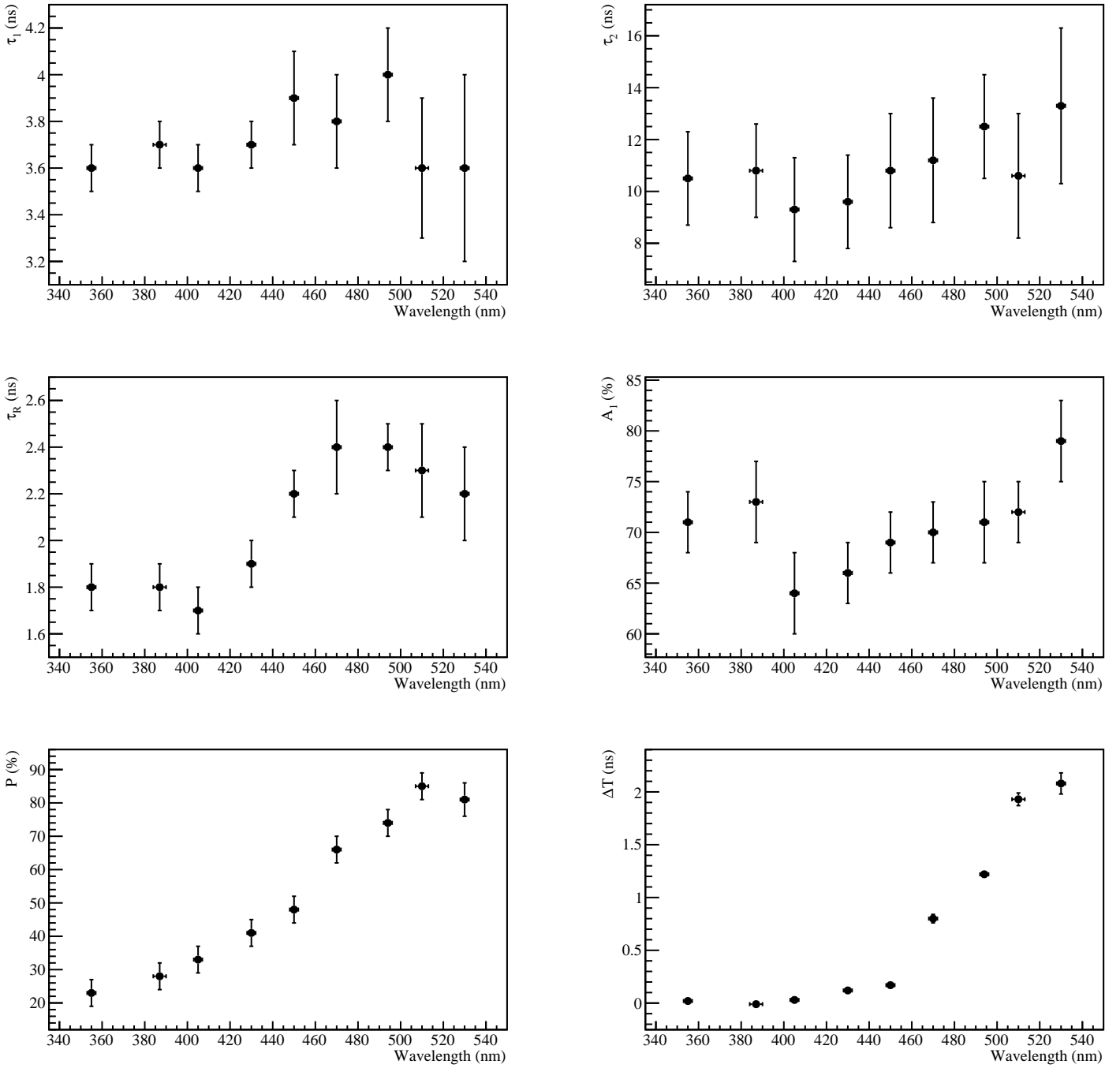


**Figure 7.** The fitted parameters defined in Equations 4.1 - 4.3. The central wavelength of the bandpass filters from Table 1 is shown plotted against the various fit parameters. These values correspond to those shown in Table 2. These plots do not include the data taken with no bandpass filter.

## References

- [1] G. D. Orebi Gann, *Physics Potential of an Advanced Scintillation Detector: Introducing THEIA*, arXiv:1504.08284 [**physics.ins-det**]
- [2] SNO+ Collaboration (S. Andringa et al.), *Current Status and Future Prospects of the SNO+ Experiment*, *Advances in High Energy Physics*, vol. 2016, 6194250
- [3] JUNO Collaboration, (F. An et al.), *Neutrino Physics with JUNO*, *J. Phys. G* 43 (2016) 030401
- [4] W. Beriguete. et al., *Production of Gadolinium-loaded Liquid Scintillator for the Daya Bay Reactor Neutrino Experiment*, arXiv:1402.6694 [**physics.ins-det**]
- [5] R. Bonventre, G. D. Orebi Gann, *Sensitivity of a low threshold directional detector to CNO-cycle solar neutrinos*, *Eur. Phys. J. C* (2018) 78: 435
- [6] S. Biller, *Probing Majorana neutrinos in the regime of the normal mass hierarchy*, *Physical Review D*, 071301R, 8 April 2013
- [7] Li Xiao-Bo et al., *Timing properties and pulse shape discrimination of LAB-based liquid scintillator*, *Chinese Physics C*. 35. 1026. 10.1088/1674-1137/35/11/009
- [8] O'Keefe et al., *Scintillation decay time and pulse shape discrimination in oxygenated and deoxygenated solutions of linear alkylbenzene for the SNO+ experiment*, *Nucl. Instrum. Meth. A* 640:119-122, 2011
- [9] T. Marrodan Undagoitia et al., *Fluorescence decay-time constants in organic liquid scintillators*, *Rev. Sci. Instrum.* 80:043301, 2009
- [10] Lombardi et al., *Decay time and pulse shape discrimination of liquid scintillators based on novel solvents*, *Nucl. Instrum. Meth. A* 701:133-144, 2013
- [11] C. Aberle et al., *Measuring Directionality in Double-Beta Decay and Neutrino Interactions with Kiloton-Scale Scintillation Detectors*, arXiv:1307.5813 [**physics.ins-det**]
- [12] M. Li et al., *Separation of Scintillation and Cherenkov Lights in Linear Alkyl Benzene*, *Nucl. Instrum. Methods Phys. Res. A* 830 (2016) 303-308
- [13] J Caravaca et al., *Cherenkov and scintillation light separation in organic liquid scintillators*, *Eur. Phys. J. C* (2017) 77: 811
- [14] L.M. Bollinger et al., *Measurement of the Time Dependence of Scintillation Intensity by a Delayed Coincidence Method*, *Review of Scientific Instruments* 32, 1044 (1961)
- [15] A. Latorre, *Lecrunch Open Source Software*, Viewed Nov. 19 2018, <https://bitbucket.org/tlatorre/lecrunch/>
- [16] Hamamatsu Photonics Datasheet, Viewed Nov. 19 2018, [https://www.hamamatsu.com/resources/pdf/etd/R7600U\\_TPMH1317E.pdf](https://www.hamamatsu.com/resources/pdf/etd/R7600U_TPMH1317E.pdf)
- [17] T. M. Undagoitia, *Measurement of light emission in organic liquid scintillators and studies towards the search for proton decay in the future large scale detector LENA*, PhD thesis, Technical University of Munich, Viewed Nov. 19, 2018
- [18] Thorlabs, *Transmission Of Bandpass Filters*, Viewed Nov. 19, 2018, [https://www.thorlabs.com/newgrouppage9.cfm?objectgroup\\_id=1860&pn=FLH355-10](https://www.thorlabs.com/newgrouppage9.cfm?objectgroup_id=1860&pn=FLH355-10)
- [19] Edmund Optics, *Transmission Of Bandpass Filters*, Viewed Nov. 19, 2018, <https://www.edmundoptics.com/p/387nm-cwl-25mm-dia-11nm-bandwidth-od-6-fluorescence-filter/27202/>

- [20] N. Barros et al., *Characterization of the ETEL D784UKFLB 11 in. photomultiplier tube*, Nucl. Instr. Meth. A852 (2017) 15
- [21] W. Verkerke, D. Kirkby, *The RooFit toolkit for data modeling*, arXiv:physics/0306116  
**[physics.data-an]**
- [22] J.B. Cummings et al., *Improving Light Yield Measurements for Low-Yield Scintillators*, arXiv:1810.02885 **[physics.ins-det]**
- [23] X. Hua-Lin et al., *Study of absorption and re-emission processes in a ternary liquid scintillation system*, Chinese Physics C, Volume 34, Issue 11, pp. 1724-1728 (2010).